

Structure in the Disk of ϵ Aurigae – Analysis of the ARCES and TripleSpec data obtained during the 2010 eclipse

Justus Gibson¹, Robert E. Stencel¹ & the ARCES team:

William Ketzeback (Apache Point Observatory), John Barentine (International Dark Sky Association), Alaina Bradley (Apache Point Observatory), Jeffrey Coughlin (SETI Institute, NASA Ames), Jack Dembicky (Apache Point Observatory), Suzanne Hawley (U Washington), Joseph Huehnerhoff (U Washington), Robin Leadbeater (Three Hills Observatory, UK), Russet McMillan (Apache Point Observatory), Gabrelle Saurage (SOFIA/USRA), Sarah Schmidt (Ohio State University), Nicholas Ule (New Mexico State University), George Wallerstein (U Washington), and Donald G. York (U Chicago).

Updated: January 11, 2017

¹ *University of Denver, Department of Physics and Astronomy*

1. Introduction

The exceptional binary star, ϵ Aurigae exhibits two year-long eclipses every 27.1 years. The eclipse of the F supergiant primary star is now understood to be caused by an opaque disk hiding a companion star (see Stencel, 2012 and references therein). An international effort to monitor all aspects of the 2009-2011 eclipse resulted in substantial archives of new data, including those involving high resolution spectroscopic monitoring, e.g. Strassmeier et al. (2014) and others. Here we report on sampling of the high resolution spectroscopic archive generated during 2009-2011 eclipse, by the ARCES instrument at Apache Point Observatory (Wang et al. 2003). As discussed by Strassmeier et al., selected spectral lines exhibit eclipse or non-eclipse behaviors, and show differential velocity effects. Our purpose is to confirm and extend their findings, in light of continuing developments about the nature of this enigmatic binary star and disk system.

Among the developments resulting from study of the 2009-2011 eclipse was recognition of third contact phenomena, interpreted as a mass transfer stream impacting the disk (Griffin & Stencel 2013). Third contact occurred during spring 2011, circa RJD 55,620 (see Stencel 2012 for eclipse contact times). Evidence for this stream was seen in low excitation Fe I lines and, curiously, lines of rare earth elements, blueshifted up to 45 km/sec. Corroborating observations of spectral line radial velocity curves near third contact, showing similar effects, were reported by Kambe et al. (2013) and Sadakane et al. (2013). Strassmeier et al. presumably would have detected similar spectral features if their robotic STELLA spectrometer had not been off-line during those portions of the eclipse. ARCES observers maintained a steady cadence through all of the eclipse phases and thus provide a more detailed picture of third contact phenomena.

In this paper we will discuss the new spectroscopic observations (Sections 2, 3 and 4), followed by an evolutionary context (Section 5), SHAPE and CLOUDY models for the system (Sections 6 and 7), and Conclusions in Section 8.

2. Observations

2.1. Description of the ARCES instrument

The ARCES instrument is an echelle spectrograph commissioned in 1999 for use with the ARC (Astrophysical Research Consortium) 3.5m telescope located at the Apache Point Observatory [<http://www.apo.nmsu.edu/arc35m/Instruments/ARCES/> - DOI: 10.1117/12.461447]. ARCES main optics consist of an off-axis paraboloidal collimator, an echelle grating, two cross-dispersing prisms, and an f/2.7 Schmidt camera with achromatic correctors. Since its commission, ARCES has been primarily used for observations of stellar abundances and as a tool for surveying diffuse interstellar bands (DIBs). Important features of this instrument include: a 2.5 pixel resolution of 31,500 (9 km/s), a spectral range of 3200Å-10000Å, an S/N ≥ 3000 , and remote operability. In addition, the efficiency of the entire telescope plus spectrograph system has been determined to be greater than 2.2% at 647nm and the spectrograph has been estimated to have an efficiency of 8% and 2% at 630nm. Some limitations of this instrument include a slight drift throughout nightly observations of about 0.5 pixels over 10 hours. This drift occurs mostly during the first half of the night and is likely due to thermal changes in the double-prism system as temperatures raise and lower. This has been accounted for by interpolating values between hourly calibrations. Overall, ARCES has been proven to be a stable, reliable instrument that has many uses in astronomical observations.

Similarly, TripleSpec is a near-IR spectrometer built for the ARC 3.5 meter telescope at Apache Point Observatory (APO: <http://www.apo.nmsu.edu/arc35m/Instruments/TRIPLESPEC/1>). Spectral coverage ranges between 0.95 and 2.46 microns, with 2.1 spectral pixel resolution of 3500 with the 1.1 arcsec slit. Steps in the data reduction described by Wang et al. (2003) include: (1) extracting spectra from raw CCD frames; (2) applying deblazing and wavelength standardization; (3) applying heliocentric RV-corrections, but no telluric corrections were attempted.

ARCES and TripleSpec observations of ϵ Aurigae are listed in Table 1, including date and Reduced Julian Date plus an estimate of the signal to noise ratio (SNR) based on continuum signal statistics as described below. To achieve high-accuracy RV measurements with the echelle spectrograph, we obtained a Thorium-Argon (Th-Ar) exposure after every science exposure. The 9 km/s velocity resolution translates to a spectral precision of 0.15Å at 5000Å and 0.20Å at 6500Å. Observations of ϵ Aurigae were obtained with ARCES beginning in 2009 Feb 16 (RJD 54878, where RJD = JD - 2,400,000) and continuing every few nights, through 2011 Dec 10 (RJD 55905). These span key times during the eclipse cycle, including ingress (2009 Aug 15, RJD 55060), second contact (2010 Feb 15, RJD 55250), mid-eclipse (2010 July 30, RJD 55400), third contact (2011 March 15, RJD 55620) and end of eclipse (2011 Aug 30, RJD 55800).

3. Data Analysis

Each spectrum obtained from the ARCES instrument was analyzed using a software tool called VOSpec. VOSpec was developed by ESA, for use in analysis and integration of spectra coming from a variety of data providers, said data having varying wavelengths and differing flux units. VOSpec

Table 1: ARCES and TripleSpec observation log for ϵ Aurigae

Date of Observation yearmonthday	RJD*	SNR	Date of Observation yearmonthday	RJD*	SNR
90216	54878	417	101213	55543	385
90311	54901	400	101216	55547	370
90408	54929	400	101220	55551	385
90410	54931	400	101226	55556	385
90412	54933	370	101229	55559	385
90413	54934	370	110104	55565	357
90414	54935	400	110108	55569	400
90505	54956	263	110114	55575	345
90729	55041	200	110121	55582	385
90804	55047	238	110205	55597	385
90908	55082	227	110211	55603	333
90924	55098	323	110214	55606	385
91002	55106	333	110222	55614	345
91027	55131	345	110304	55624	357
91031	55135	345	110307	55627	270
91105	55140	345	110316	55636	303
91108	55143	357	110320	55640	303
91118	55153	357	110329	55649	313
91126	55161	333	110401	55652***	323
91207	55172	370	110402	55653	323
91220	55185	370	110406	55657	161
91225	55190	385	110413	55664	323
100101	55197	385	110416	55667	333
100104	55200	213	110428	55679	357
100111	55207	417	110503	55684	345
100117	55213	357	110729	55771	179
100130	55226	370	110802	55775	244
100213	55240	417	110805	55778	128
100225	55252	345	110813	55786	161
100307	55262	294	110823	55796	217
100308	55263	286	110827	55800	58
100312	55267	435	110831	55804	217
100322	55277	400	110920	55824	250
100331	55286	370	110924	55828	286
100407	55293	345	111007	55841	286
100410	55296	417	111011	55845	278
100424	55310	303	111016	55850	313
100425	55311	270	111023	55857	286
100427	55313	303	111026	55860	278
100722	55399**	161	111030	55864	313
100811	55419	196	111102	55867	263
100821	55429	189	111104	55869	263
100905	55444	294	111107	55872	196
100912	55451	294	111111	55876	294
100924	55463	333	111116	55881	286
100929	55468	323	111119	55884	270
101007	55476	345	111129	55894	270
101011	55480	323	111210	55905	345
101015	55484	345	111216	55911	345
101018	55487	313	111228	55923	323
101026	55495	333	120101	55927	125
101029	55498	385	120106	55932	357
101103	55503	370	120113	55939	278
101107	55507	357	120131	55957	357
101108	55508	385	120209	55966	141
101111	55511	370	120214	55971	345
101116	55516	400	120305	55991	345
101120	55520	357	120323	56009	370
101122	55522	345	120406	56023	313
101124	55524	323	120409	56026	167
101204	55534	182	120428	56045	294
101209	55539	370			

*RJD = J.D. - 2,400,000. **Close to mid-eclipse. ***Close to third contact.

has many tools built into the program such as line fitting, redshift corrections, as well as the ability to calculate equivalent widths and radial velocities. In order to determine the overall quality of each spectrum, a standard deviation function was applied in VOSpec for the featureless continuum between two Si II lines at 6347Å and 6371Å. This interval appears relatively free of any telluric or stellar features. Thus, determining the standard deviation of the continuum gives a measure of the signal-to-noise ratio of each spectrum. To do this, a range was manually selected in VOSpec ranging from approximately 6350Å to 6368Å and then the standard deviation function was applied to the selected region. The results of these tests can be seen in Table 1, reported as SNR, which is the inverse of the continuum interval standard deviation, assuming the usual statistics. The majority of the spectra have SNR in excess of 200.

3.1. Selected absorption lines in ARCES spectra of ϵ Aurigae

Based on previous work, we have elected to study the following spectral lines and obtained their atomic properties from the online NIST Atomic Spectra Database (Table 2).

3.1.1. High excitation lines of Si II and Fe II

VOSpec was used to calculate wavelength minima which were, in turn, used to calculate radial velocities of certain Si II, Fe I, and Fe II spectral lines (Strassmeier et al. (2014)). The equivalent width function and the line velocity measurement of VOSpec work by selecting a wavelength range for a particular line of interest and then applying the equivalent width function. For line velocities, the minima of each line was determined and then a Doppler velocity calculation was performed to deduce the radial velocity. The Si II behavior will be referred to as a *Type 1* variation where we see a gradual decrease in radial velocity from +10km/s to -15km/s over a 1200 day period giving an deceleration of 0.021 km/s/d (Figure 1). The measured equivalent width of 0.57 ± 0.03 Å suggests that despite the velocity changes, the integrated line formation regions are largely unchanged with time.

Velocity variations in Fe II 6417 + 6432 are similar to Si II (Figure 1) with the exception of a large, negative spike at third contact (RJD 55600), during which a secondary profile component was present. The equivalent widths are essentially unchanged despite the variations in velocity. Additional pairs of high energy lines are the Mg II 4481Å and Fe II 6417/6432Å lines with velocity variations similar to Si II.

In contrast, H β shows a lot of variation in velocity and equivalent width (Figure 2). We interpret this as revealing mostly disk rotation combined with F-star orbital motion. This is a *Type 2* variation characterized by a velocity decrease from 20 km/s to 50 km/s over a period of 400 days around mid-eclipse, giving a deceleration of 0.075 km/sec/day, or 8.68×10^{-4} m sec $^{-2}$.

Figure 3 shows the velocity variations observed in the Fe II 4629.33Å line, revealing a complex interplay of several dynamically significant features in the disk. By measuring the progression of each feature appearing and associated with this line (and others), we can trace the following three

Table 2: Atomic line parameters

Species	Rest Wavelength, Å	Multiplet, eV lower	f-value	Reference
Un-	eclipsed	lines		
Mg II	4481.130	2D 5/2-2Fo 7/2, 8.86	0.935	SE
Mg II	4481.327	2D 3/2 - 2Fo 5/2, 8.86	0.981	SE
Fe I	5615.6	z5Fo-e5D, 3.33	0.010	k
Si II	6347.10	2S-2Po, 8.12	0.705	s, k
Si II	6371.36	2S-2Po, 8.12	0.414	s
Fe II	6417.46	3d6-y2Fo, 8.63	–	–
Fe II	6432.68	3d6 - 4P, 10.93	0.015	–
Eclipsed	lines			
Fe I	4132.06	a3F-y3Fo, 1.61	0.042	s
Fe II	4178.86*	b4P-z4Fo, 2.58	6E-4	s
blend	Cr I 4179.43			
Fe I	4202.03	a3F-z3Go, 1.48	0.022	s
Fe II	4303.18	b4P-z4Do, 2.70	6E-4	s
Ti II	4468.492	a2G9/2 - z2Fo7/2, 1.13	0.024	SE
Fe II	4555.89	b4F-z4Fo, 2.82	7E-4	s
Fe II	4629.33	b4F-z4Fo, 2.81	6E-4	s
Fe II	4923.92	a6S-z6Po, 2.89	0.010	s,k
Fe I	5110.4	a1H-z1Ho, 3.57	0.000	k
Fe I	5168.90	a5D-z7Do, 0.05	1.5E-5	s
Fe II	5169.03	a6S-z6Po, 2.89	0.023	s
Fe I	5169.29	c3F-t3Do, 4.07	–	s
Fe II	5169.80	f4D-2[3]o, 10.50	0.008	s
Fe I	5615.64A	z5Fo5 - e5D4, 3.33	0.10	k

Data from <http://physics.nist.gov/PhysRefData/ASD/lines>

s = Strassmeier et al. 2014; k = Kambe et al. 2013; SE = Struve and Elvey 1930

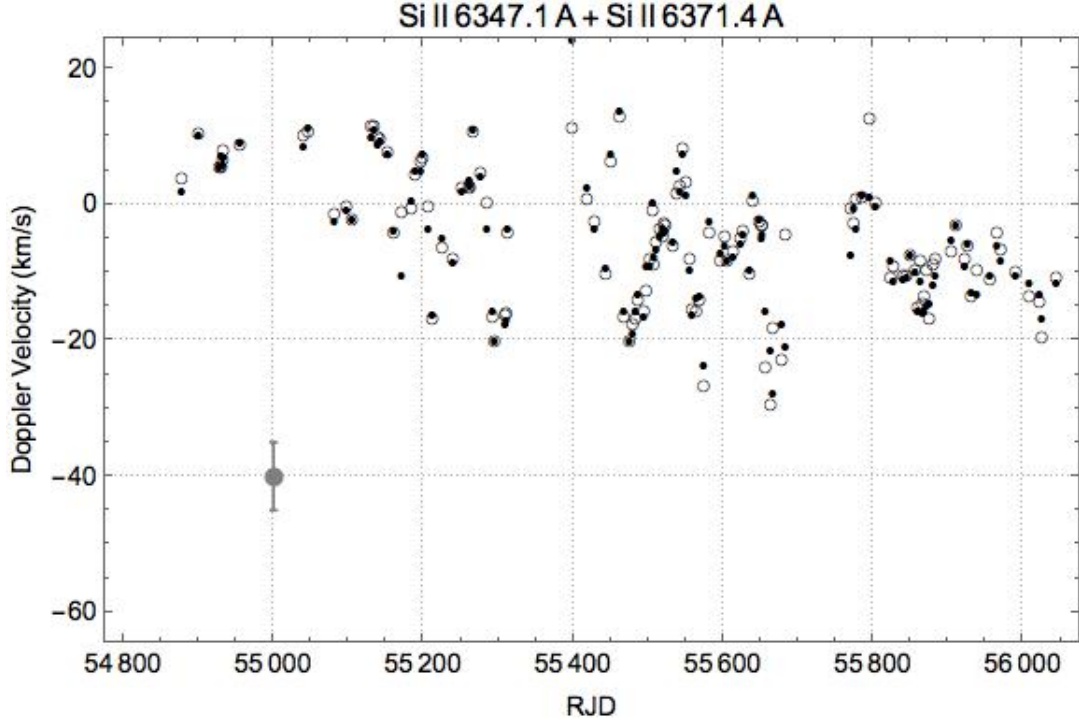


Fig. 1.— Si II 6347.1Å and Si II 6371.4Å velocity represented by open and closed circles, respectively. The velocity variations are typical of out of eclipse variations associated with non-radial oscillations of the F star photosphere.

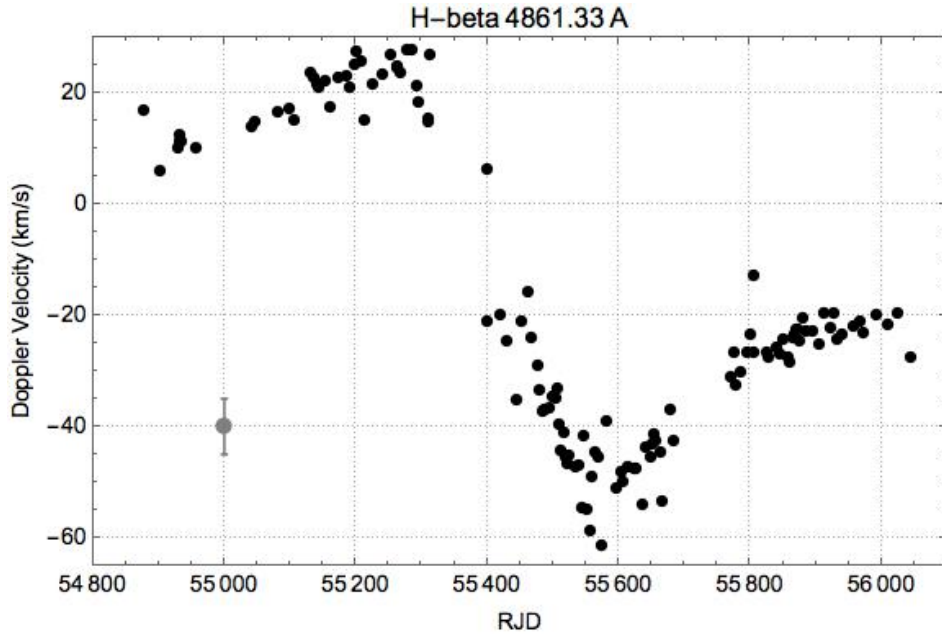


Fig. 2.— Radial velocity of flux minima in $H\beta$, an optically thick line, showing a simple velocity variation interpreted as disk rotation.

features: (1) a lower amplitude, sinusoidal variation during eclipse - redshifted to ~ 15 km/sec near second contact, then blueshifted to ~ -10 km/sec near third contact; (2) a higher amplitude variation, initially indistinguishable from (1) until after second contact, but then reaching ~ -40 km/sec near third contact, and (3) a dramatic but short lived extreme blue-shifted feature only at third contact, appearing close to -60 km/sec but merging with feature (2) soon thereafter.

We interpret these three features as follows: the upper curve represents the F star orbital motion (amplitude a few km/sec), while the middle curve represents rotation of a disturbed portion of the disk (amplitude tens of km/sec), perhaps related to the extra feature near RJD 55600 - the impact of a mass transfer stream, briefly illuminated by the background F star during third contact. This third feature is the mass transfer stream, discovered by Griffin and Stencel (2013) but not revealed with this degree of detail, prior to ARCES coverage. Velocity curves presented by Strassmeier et al. (2014) drew our attention to these high velocity features, but their temporal coverage was limited by instrument downtime, close to third contact. We posit that the low and high eccentricity lines as described by Strassmeier et al. are defined by variations of type 1 and type 2, respectively, in our nomenclature. Variation of type 3 is the disrupted portion of the disk, caused by stream impact primarily near azimuths around third contact. This is a *Type 3* variation characterized by the the Type 2 sine variation plus an extra infall stream at RJD 55600-55700 (acceleration = 0.27 km/s/day, or 3.13×10^{-3} m sec $^{-2}$. with opposite sign and ten times larger than the $H\beta$ value shown in Figure 2.

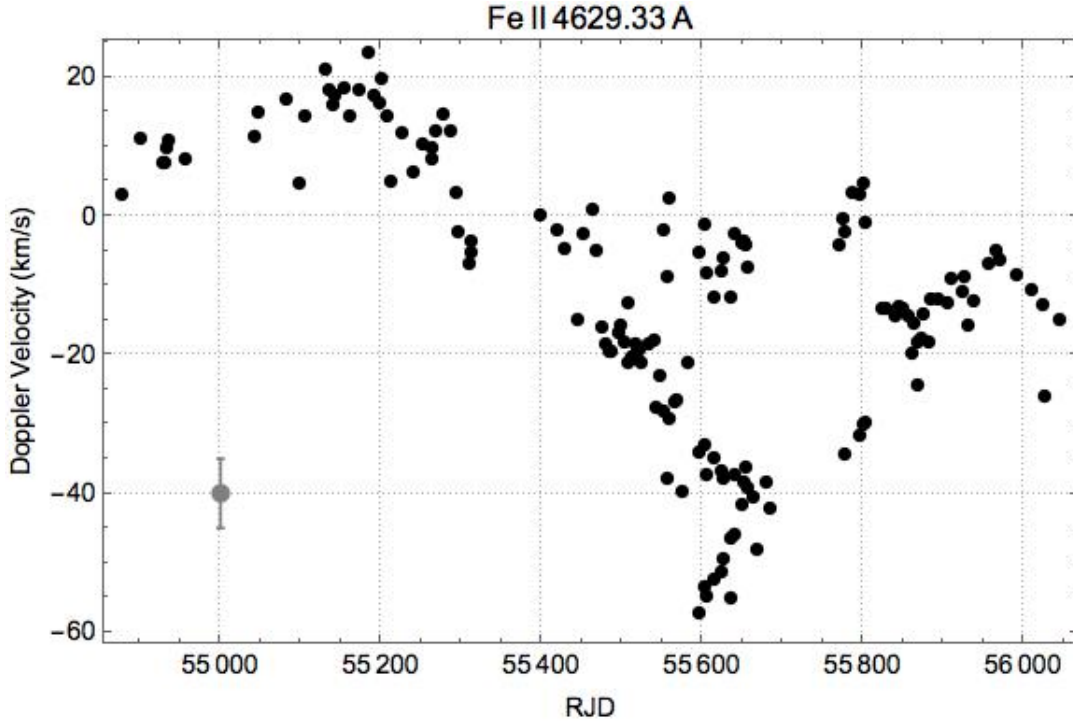


Fig. 3.— Radial velocity of flux minima in Fe II 4629Å. Unlike $H\beta$, we see the same sine curve as well as another branch, near zero velocity, prominent after mid-eclipse, and we also observe a third contact high velocity component, prominent at RJD 55600.

3.1.2. *Velocity Changes of Selected Disk/Stream Sensitive Lines*

Sadakane et al. (2013) identified a series of lines that showed clear changes due to the passage of the disk. Their radial velocity plots show several lines, identified in Table 2 and discussed below, with extreme blueshifts during third contact times, but with late eclipse coverage gaps in their robotic series. We report two kinds here: those showing disk motion, and those showing disk plus stream motions. First, the disk-only set of lines, typically having the lowest excitation potentials (less than 2 eV) and not showing velocities much in excess of -40 km/sec, for example $H\beta$ in Figure 2. The hydrogen lines are optically thick and sensitive to larger scale phenomena in and around the disk and the F star wind (Mourard et al. 2012). The second group of lines show the disk motion, plus evidence for an infall stream, close to third contact (RJD 55,600), with velocities around -60 km/sec (see Figure 3).

3.1.3. *Line Profile Evolution of Selected Lines*

In order to better understand the spectral lines that have been shown to have disk absorption during mid-eclipse (Strassmeier et al. 2014), certain lines (see Table 2) were evaluated for their velocity changes. Some lines showed the formation of doublets around RJD 55399 such as the iron blend line at 5169.1Å and 5169.3Å (Figure 5). The line is unshifted until just before first contact where a noticeable redshift begins and peaks around RJD 55200. On RJD 55399, clear doubling has begun in the line which persists and strengthens until after fourth contact. Right before third contact begins, the line begins to show blueshifting that persists all the way through fourth contact.

Another line studied in detail was the Fe II line at 4629.33Å, which traces the mass transfer stream the best as seen in Figure 4. As can be seen, line tripling persists through most of the third contact with the highest velocity occurring around RJD 55606. By the end of third contact the line is only doubled tracing background star and disk, but losing the contribution from the mass transfer stream. Also of note is the extreme blueshift that begins to occur around mid-eclipse and peaks through third contact. The iron line 5110.4Å was also examined in detail because of the third-contact line strengthening observed. As can be seen in Figure 6 the line is mostly non-existent before and after third-contact, but strengthens significantly during third contact showing strong blueshifted absorption with velocities up to -60 km/sec.

In order to illustrate the significant differences over time we have explored differentials between spectra and averages of those spectra, using the principles of singular value decomposition (SVD) and/or principal component analysis (PCA) – see Skumanich & Lopez-Ariste (2002) and Casini et al. (2005). The principal component analysis was performed by first averaging the wavelengths and intensities of all epochs in our data set, for the case of 5169.3Å, or by only averaging the first three and last three dates in our data sets as in the cases of 4629.33Å and 5110.4Å. Once an average line profile was obtained, a ratio was taken between the average line profile and each individual line profile in our range of dates. These results were plotted against radial velocities of each line with zero velocity being defined as the rest wavelength of the line. The results are shown alongside evolution plots in Figures 4-6.

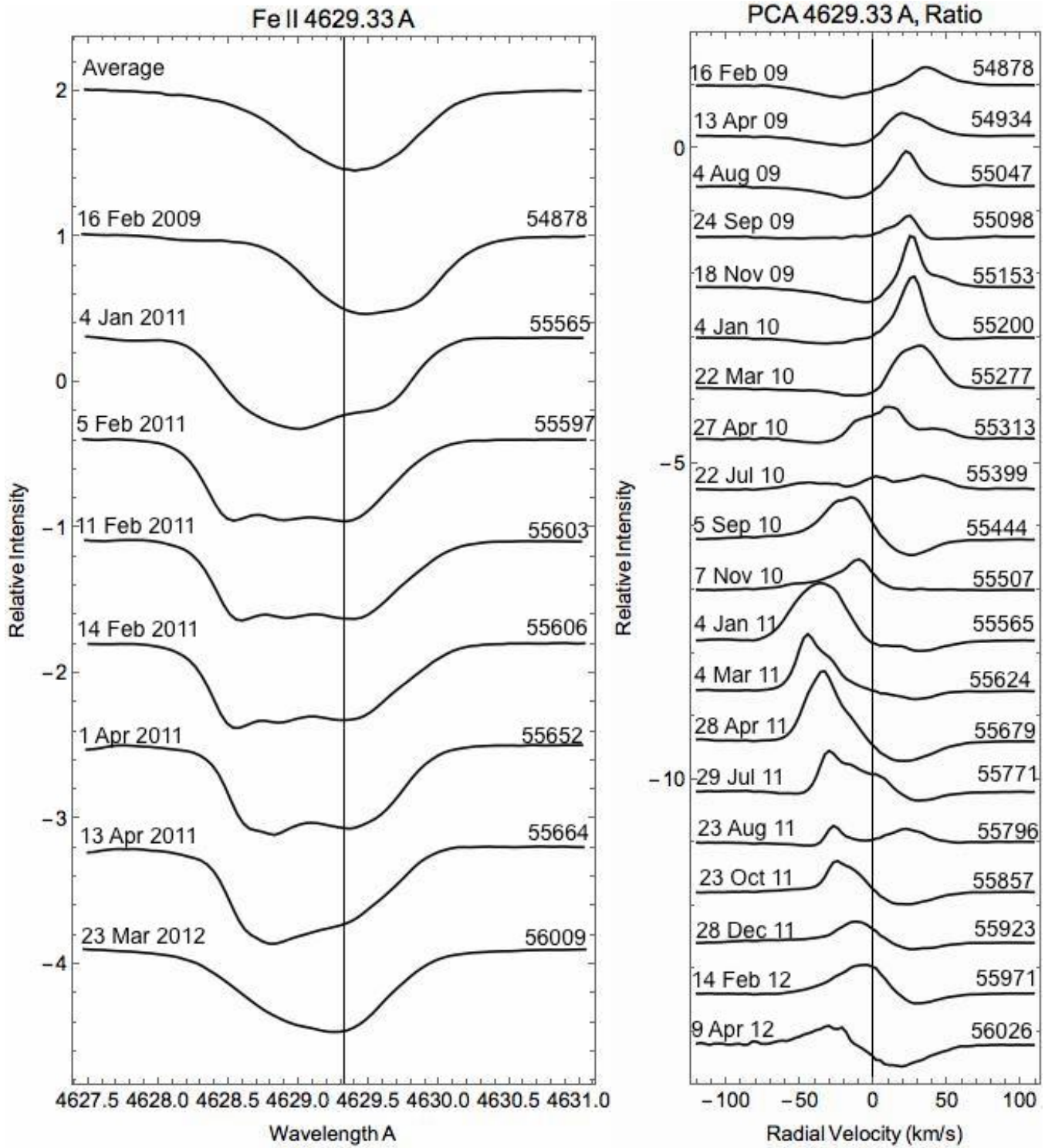


Fig. 4.— This figure shows the evolution of the Fe II line at 4629.33 Å (2.81 eV). The left-most figure shows the intensity evolution around third contact clearly showing three minima that are representative of the background star, disk, and the mass transfer stream. Seven epochs were chosen to bring out details in the high-velocity, third contact material. The right-most figure shows the results of a first-order principal component analysis on 4629.33 Å where the average was obtained from the first three and last three spectra (out of eclipse phases) in our data set. For reference, the averaged spectrum is at the top of the left-most figure.

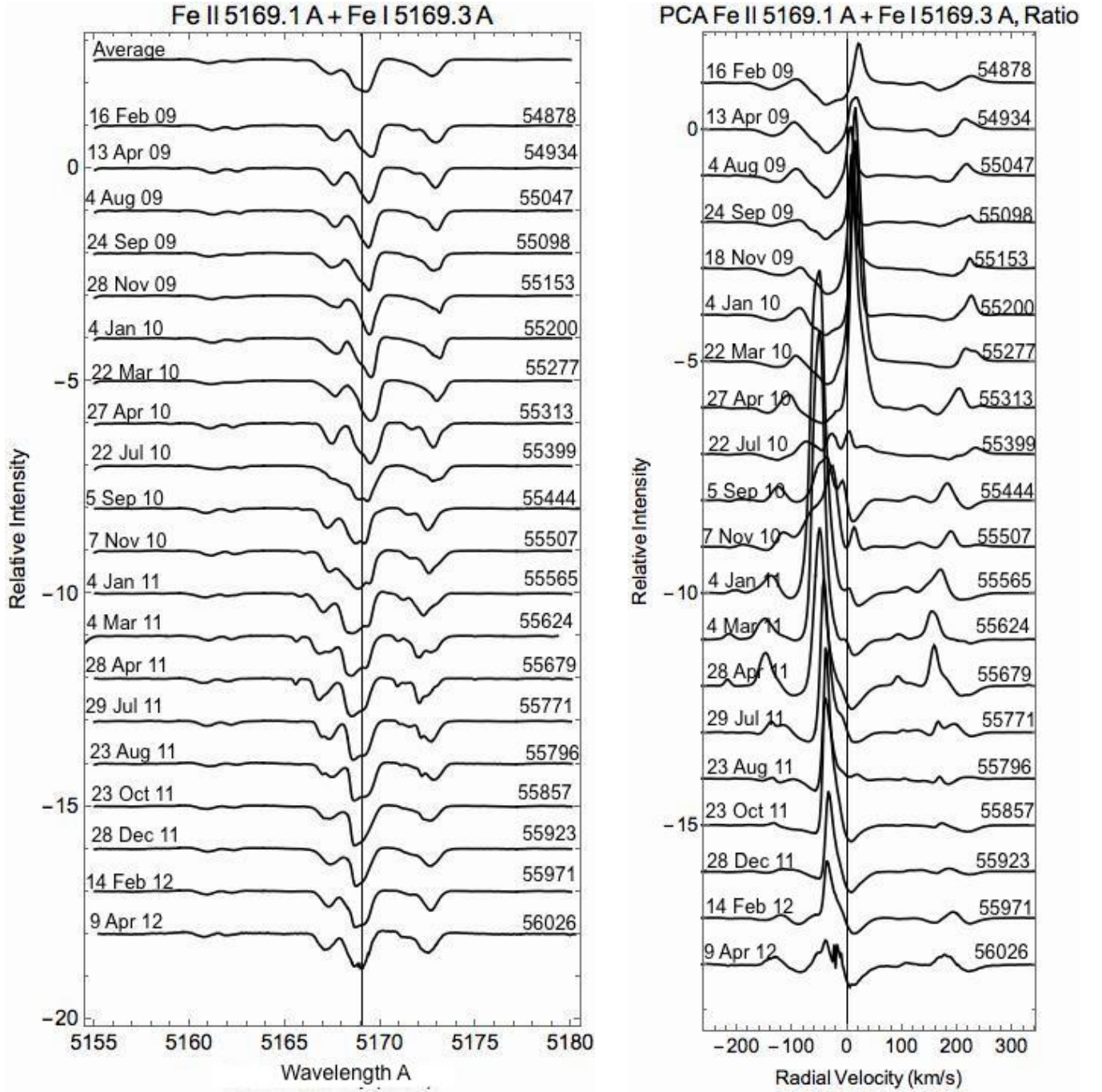


Fig. 5.— This figure on the right shows a multiplot of Fe II 5169.03 Å (2.89 eV) with dates spanning the whole period of monitoring of the eclipse. As can be seen, Doppler redshift becomes prominent around second contact (RJD 55200) whereas near mid-eclipse (RJD 55480) we begin to see line-doubling and blue-shifting of the central line. The right-most figure shows the results of a first-order principal component analysis on the iron blend where the average was obtained from all of the chosen dates. Again, the averaged spectrum over all dates is shown for reference at the top of the left-most figure.

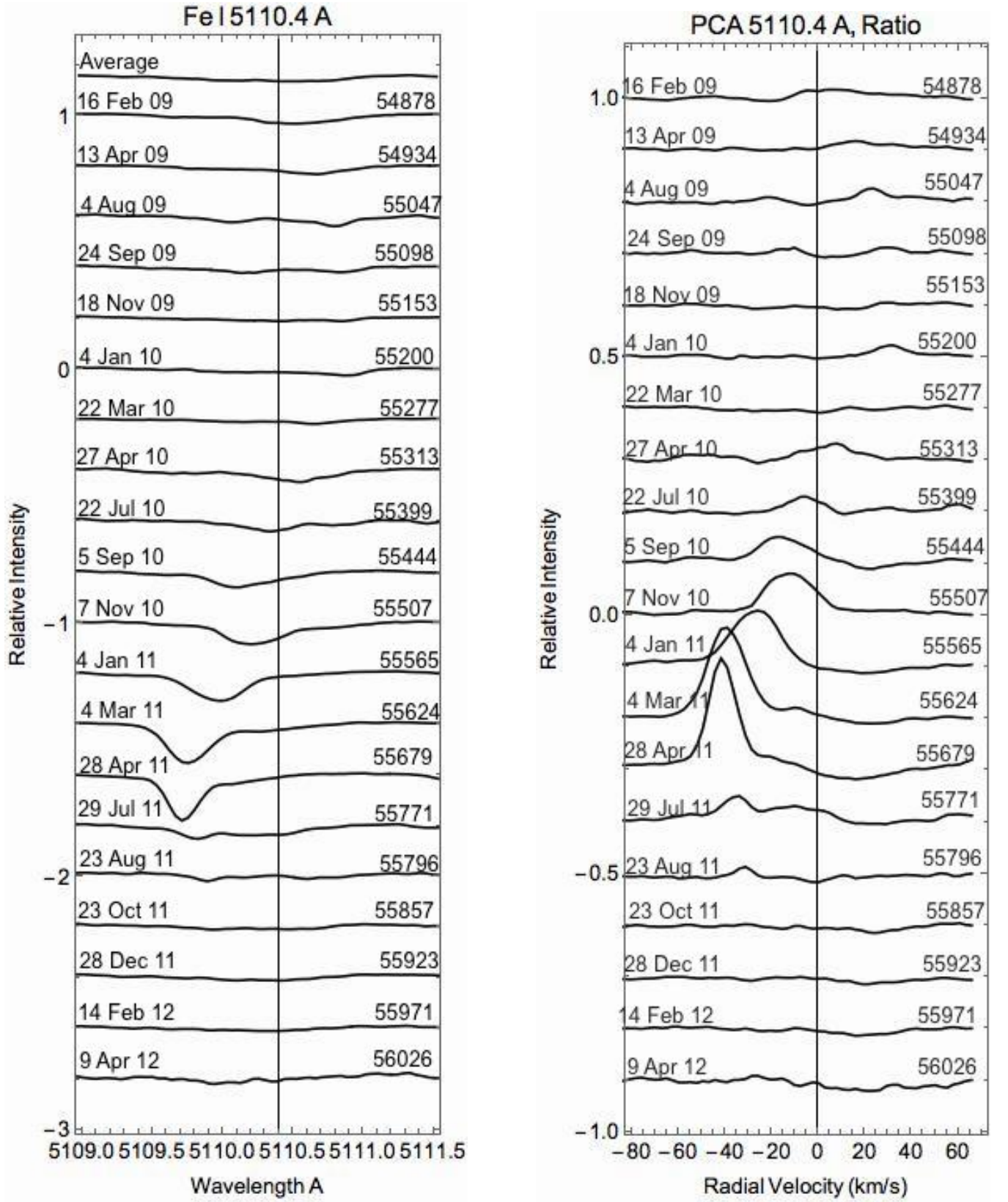


Fig. 6.— Comparison between line evolution and a first-order ratio PCA for the line at 5110.4 Å (3.57 eV) similar to Figures 4 and 5. The average shown at the top of the left-most figure was obtained from the first three and last three spectra in our data set.

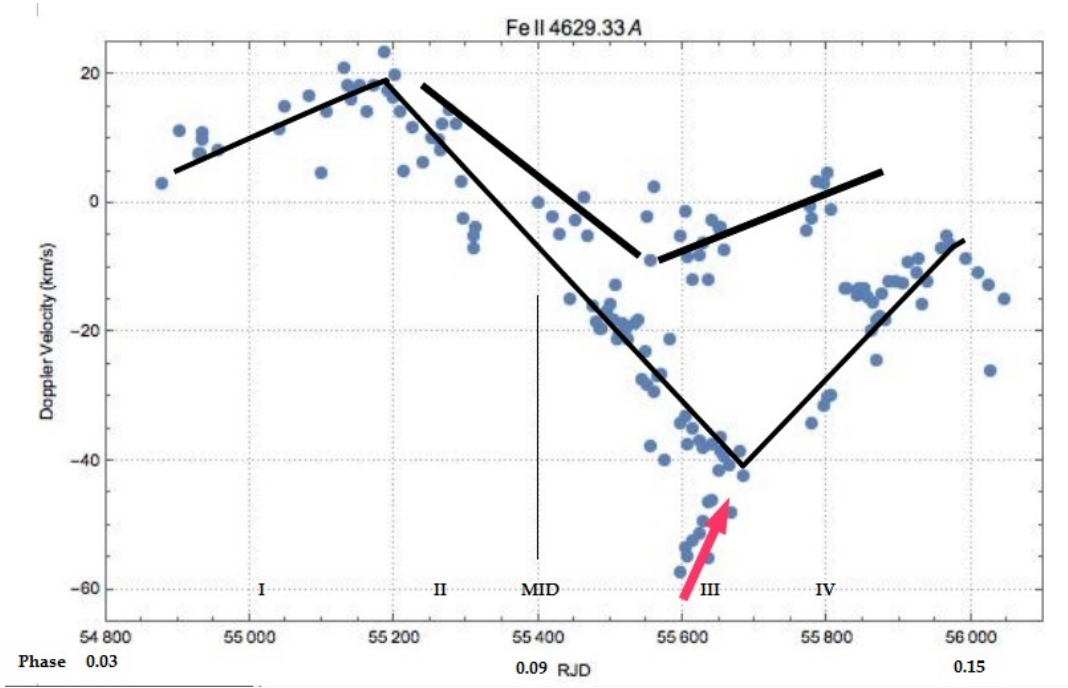


Fig. 7.— This graph shows an interpretation of the velocities of flux minima within the Fe II line at 4629.33Å, plotted against reduced Julian date. See text for details.

4. Discussion

As shown in Figure 7, we posit that the low and high eccentricity lines as defined by Strassmeier et al. are defined by variation types 1 and 2, respectively, in our nomenclature. Type 3 is the disrupted portion of the disk, caused by stream impact primarily among azimuths near third contact.

These sets of velocities define the energetics and must be shown to be consistent with a binary star mass ratio, once that gets determined. Meanwhile, we consider the following estimates: adopting a $6 M_{\odot}$ B star at the center of the disk, and an outer disk radius of 4AU as defined by the CHARA+MIRC interferometric observations, the Keplerian speed of the outer disk should be 36 km/sec, which is about that seen in type 2 variation. The 60 km/sec represents a terminal velocity of material accelerated toward the B star from a large distance (e.g. the inner Lagrangian point), only ~ 6 AU distant, using these numbers. The rate of deceleration (-60 to -40 km/sec) over a span of ~ 50 days is a result of ballistic infall of material from the inner Lagrangian point and collision with transverse disk material.

5. Evolutionary Models

In order to better understand and make predictions about the masses and evolutionary future of Epsilon Aurigae, a multi-parametric chi-squared minimization was performed, similar to the method described by Mennickent et al. (2014). Comparing previously observed quantities, the

temperatures and luminosities of both components as proposed by Hoard et al. (2010), with those predicted by van Rensbergen et al. (2011) models of conservative and non-conservative binary star evolution, we were able to seek models that best fit the observed data. Higher initial mass models are required to reach the F star log luminosity of 4.5 or higher. One interesting model is 09strong that features initial masses of 9 and 8.1 solar masses ($q=1.11$), which evolve into a post-mass exchange 2.97 and 13.54 solar mass pair at $t=32.8$ Myr, dwelling there until end of calculation, when $t=32.82$ Myr and masses have changed to 3.2 and 14.11 solar masses ($q=0.23$) at virtually the same luminosity for the originally more massive star ($\log L = 4.1$, $\log Te = 3.875$).

Table 3: Van Rensbergen Evolutionary Model

Model	M1	M2	t(Myr)	P(days)
09strong	9.0	8.1	0	20
09strong	3.11	13.05	32.794	144
09strong	2.31	14.11	32.839	163

6. SHAPE Visualization of Disk and Stream

SHAPE 5.0 is a morpho-kinematic modeling and reconstruction tool used for astrophysical objects. With SHAPE, users can input any known physical parameters of their objects and can augment single bodies with clouds, disks, and other features. It is also possible to specify chemical abundances as well as emission and absorption lines. Automatically created with each physical model is a velocity-space model, as well as a graph of the object’s velocity curve. Users also have the capability to change the frame through which the object is being viewed, by changing inclination and by rotating the object with respect to the observer. One problem with SHAPE was the tendency for files to be unsaved or deleted in between opening and working with them.

SHAPE was used to interpret and model the mass transfer stream observed during third contact. A small sphere was set in the center of the frame and surrounded by a disk, representing the B star and the accretion disk. The primary F star is set in the background at roughly third contact and there are two separate "clouds" representing the observed mass transfer stream. The cloud farther out from the disk represents the higher velocity component that is illuminated by the F star first, and then transitions into the slower, closer in cloud as the eclipse ends. The deceleration from -60 km/s to -40 km/s over the projected distance of one F star radius is indicative of an 8 solar mass central star inside the disk, assuming the disk radius scale derived by Kloppenborg et al. (2015) at the 737 pc distance. The mass function implies an F star mass of 6 solar masses ($q=0.78$). For the 1 kpc distance, the implied mass inside the disk is 11 solar masses, and for the F star, 12 solar masses ($q = 1.1$).

One challenging aspect of the stream velocity at third contact is why it only appears between RJD 55600 and 55650, which is only 0.3 percent of the orbital phase. This suggests the higher speed stream closely parallels the edge of the opaque disk. Broadband polarization reported by

Kemp et al. (1986) spikes after mid-eclipse and during third contact, which suggests strong forward scattering of light by circum-disk material during those phases.

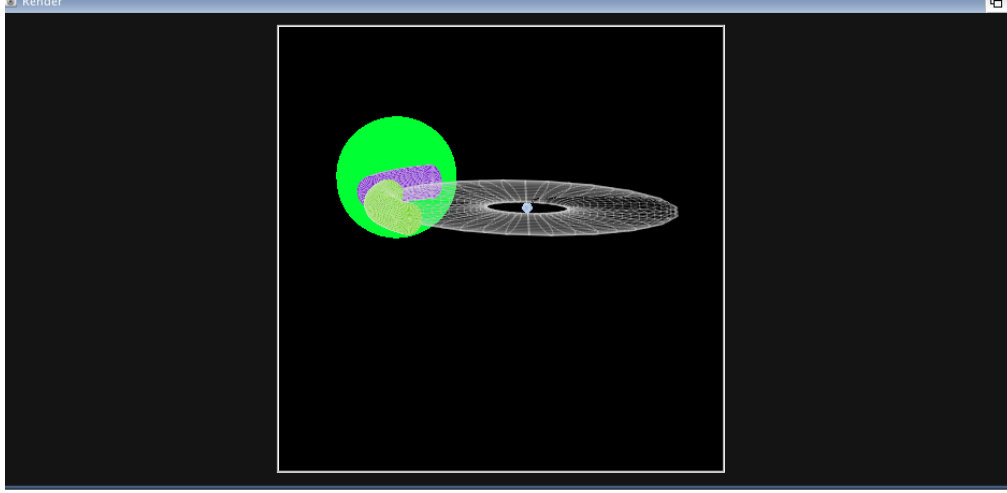


Fig. 8.— SHAPE software visualization of the disk with the stream component representation at third contact projected against the background F-star. The inclination of the system has been set at 80 degrees for the purpose of clarity.

7. Spectral Line Modeling with CLOUDY

7.1. TripleSpec Observations of He I 10830 Å Lines and Pa- β

In addition to the optical spectra obtained by ARCES, described above, a co-mounted near-infrared spectrograph captured data on the same schedule (Table 1). TripleSpec provides wavelength coverage from 0.95 to 2.46 microns with a spectral resolution of 3500 using the 1.1 arcsec slit.

Previously reported changes in the Helium I 10830Å line (Stencel et al. 2011) reveal a large increase in absorption equivalent width during mid-eclipse. The more extensive coverage with TripleSpec confirms this behavior and enables study of details of the mid-eclipse, per Figure 9, including a suggestion of a local minimum near RJD 55475, roughly 1 AU past mid-eclipse. This offset could relate to the position of the disk inner wall.

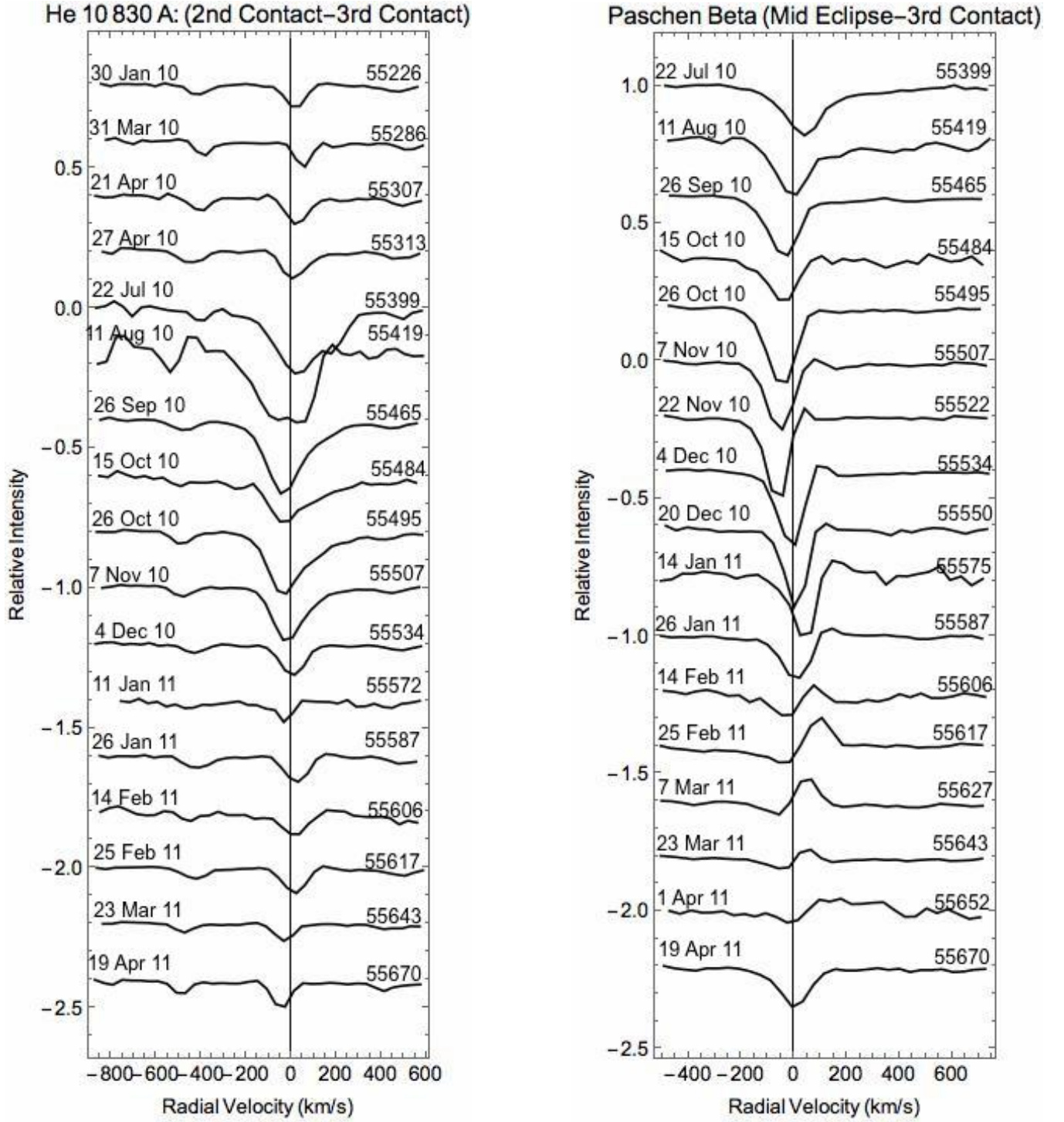


Fig. 9.— Variation of equivalent width of the He I 10830 Å line during the eclipse of ϵ Aurigae, as seen with TripleSpec. Variation of the Pa β line profile during third contact phase of the eclipse of ϵ Aurigae, as seen with TripleSpec.

Equally interesting was the appearance, starting after mid-eclipse and especially during third contact, of a P Cygni profile in the Paschen β line at 1.28 microns. The blue-edge velocity is approximately 100 km s^{-1} , presumably arising from the energetics due to the stream - disk collision.

7.2. CLOUDY models

CLOUDY is an internationally used spectral synthesis code designed to simulate conditions in plasmas, such as circumstellar and interstellar matter, exposed to a radiation field under a broad range of conditions. CLOUDY also has the ability to predict emission and absorption spectra, which can be compared with the observed data. Extending over the whole electromagnetic spectrum, CLOUDY includes the 30 lightest elements in its calculations and the relative concentrations of these elements can be modified. The ionic and molecular emission data used in CLOUDY comes from the CHIANTI database, the LAMDA database as well, as its own atomic and molecular Database with level energies taken from NIST (Turner et al. 2016). For our purposes, CLOUDY was used to interpret the equivalent widths of two lines that experienced broadening and strengthening during the eclipse: He 18030Å and H- α .

To generate equivalent widths from the CLOUDY code, certain parameters had to be specified in order to generate a continuum file that would contain the calculated intensities over our selected range of wavelengths. For the input parameters we varied log temperature and log density, to see their effect on the line strength, while other parameters such as geometry, radius, and chemical abundances were not varied. Temperature was run from 15000K to 30000K with a step size of 2500K, or in log terms, from 4.17 to 4.47. The log of the hydrogen density was varied from 8 to 12 with a step size of 0.5. For our code, we assumed an open geometry with an inner and outer radius set at 1AU and 5AU, respectively. Chemical abundances were assumed to be the same as solar abundances (Grevesse et al. 2010). The code was iterated twice and the continuum results were exported to a text file. Equivalent width was plotted as a function of log density and log temperature as can be seen in Figures 10 and 11. The blue space shows the deviation from the observed maximum equivalent width of Helium I 10830Å which was 2Å. A determination for disk density was given by Stencel et al. (2015) by fitting transient CO lines seen near third contact. The result was that $\log n = 10.5$. Figures 10 and 11 suggest that for $\log n = 11$ then $T=15000K$ provides a 'good' fit for the equivalent width of both He 10830 and for H- α . We conclude this temperature is consistent with a B5V central star.

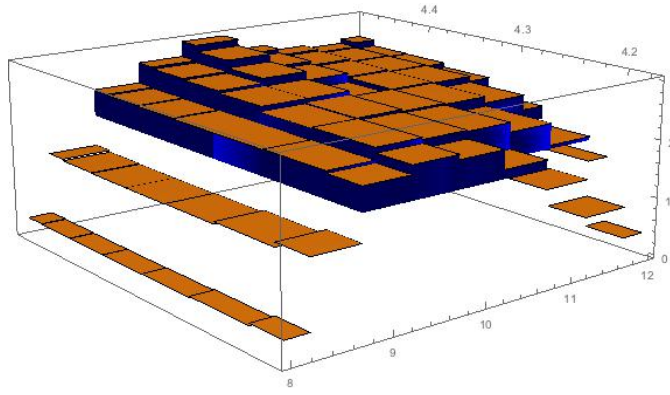


Fig. 10.— A 3-Dimensional image showing how the equivalent width of He 10830Å varies with different densities and temperatures. Temperatures were run from 15000 K to 30000 K, with a step-size of 2500, and the log of the hydrogen density ranged from 8 to 12 cm^{-3} , with a step-size of 0.5.

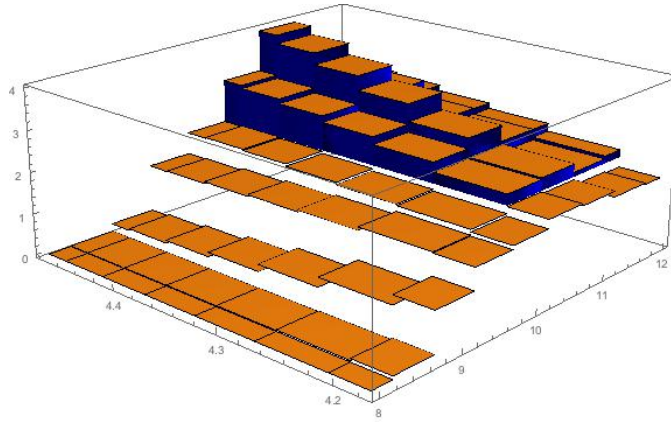


Fig. 11.— A 3-Dimensional image showing how the equivalent width of H- α varies with different densities and temperatures. Temperatures were run from 15000 K to 30000 K and the log of the hydrogen density ranged from 8 to 12 cm^{-3} .

8. Conclusions

Spectroscopic monitoring of ϵ Aurigae during its recent eclipse, using the Apache Point Observatory ARCES and TripleSpec instruments, has helped detail substructure in the disk and stream at selected phases. In particular, the amplitude of the disk velocity is better defined and the appearance and velocity of the stream is more well defined. Variations in the He I 10830Å absorption line strength during mid-eclipse was shown to relate to the inner disk structure. Hydrogen Pa β exhibits a P Cygni profile during third contact, suggestive of an expansion zone related to stream impact zone. Having defined special phases around third contact, ideally more targeted observations can be arranged during the next third contact time-frame, in particular (RJD 65510 or 2038 March 28).

One hope resulting from study of these data is another attempt to determine the distance to the ϵ Aurigae system - much debated in the literature. Recent work by Guinan et al. (2012) claimed to constrain distance estimates to 1.5 ± 0.5 kpc, using correlations between distance measurements to stars in the vicinity of ϵ Aur with interstellar absorption and reddening properties. However, that study rests on several assumptions, including uniformity of the interstellar medium (ISM), enforcing strictly linear correlations between distance-sensitive properties, and spectral type calibration uncertainties that factor into their MESA models and distance moduli. Distances based on different DIBs disagree with each other, so reliance on a single one also can be highly suspect Friedman et al. (2011). Each of these assumptions contribute to a substantial cumulative uncertainty in their distance estimate. It is instructive to note that several binary stars exist in the ϵ Aurigae field. For example, B-type stars are fairly common within a few degrees, and indications are that the ϵ Aurigae primary could have arisen from a B-type main sequence star, and its disk may contain a B-type secondary star. Similarly, ϵ Aurigae has a moderate eccentricity $e = 0.227$ Stefanik et al. (2010). Two neighbor stars, which also are Guinan et al. sample stars, turn out to be high eccentricity B-star binaries. These stars are HD 31894 ($e=0.61$, estimated stellar mass of $9M_{\odot}$) and HD 31617 ($e=0.76$, estimated primary stellar mass of 9 to $15M_{\odot}$). The formation of such binaries represents a challenge to star forming theories. Another neighbor, HD 30353 (A5Iap), is suggested to be a Case C mass transfer binary (Lauterborn 1970). Collectively, are these clues to binary star evolution in this region of our galaxy? We argue that this may be so, and explore the implications thereof. The distance moduli for these B star binaries and angular proximity to ϵ Aurigae argue for a distance less than 1kpc.

Acknowledgements: This work was supported in part by the bequest of William Herschel Womble in support of astronomy at the University of Denver. J.G. thanks the University of Denver Undergraduate Research Center for a Partners in Scholarship (PinS) grant, and the Native American Scholarship fund that helped his efforts in this research. The authors are grateful to the Astronomical Research Consortium (ARC) that operates the Apache Point Observatory 3.5 meter telescopes and its ARCES and TripleSpec instruments that provided the bulk of the data reported in this paper.

9. References

- Casini, R.; Bevilacqua, R.; Lopez Ariste, A., 2005. ApJ, 622, 1265. Principal Component Analysis of the He I D3 Polarization Profiles from Solar Prominences. <http://adsabs.harvard.edu/abs/2005ApJ...622.1265C/>
- Friedman, Scott D.; York, Donald G.; McCall, Benjamin J.; Dahlstrom, Julie; Sonnentrucker, Paule; Welty, Daniel E.; Drosback, Meredith M.; Hobbs, L. M.; Rachford, Brian L.; Snow, Theodore P. 2011. The Astrophysical Journal, 727, 1. Studies of Diffuse Interstellar Bands V. Pairwise Correlations of Eight Strong DIBs and Neutral Hydrogen, Molecular Hydrogen, and Color Excess. <http://adsabs.harvard.edu/abs/2011ApJ...727...33F>
- Griffin, R.E.M. and Stencel, R.E. 2013 PASP 125, 775. Merging Recent and Historic Spectra of Aurigae: Properties of the System's Components, and Discovery of a Mass Transfer Stream.

<http://adsabs.harvard.edu/abs/2013PASP..125..775G>

- Grevesse, N.; Asplund, M.; Sauvahttp://adsabs.harvard.edu/abs/2011ApJ...727...33Fl, A. J.; Scott, P. 2010, *Astrophysics and Space Science*, Volume 328, Issue 1-2, pp. 179-183, The chemical composition of the Sun. <http://adsabs.harvard.edu/abs/2010ApSS.328..179G>
- Guinan, E. F.; Mayer, P.; Harmanec, P.; Boi, H.; Bro, M.; Nemravov, J.; Engle, S.; lechta, M.; Zasche, P.; Wolf, M.; Korkov, D.; Johnston, C. 2012. *Astronomy and Astrophysics*, Volume 546, id.A123. Large distance of Aurigae inferred from interstellar absorption and reddening <http://adsabs.harvard.edu/abs/2012A%26A...546A.123G>
- Hoard, D. W.; Howell, S. B.; Stencel, R. E. 2010 *Astrophys. Journal* 714, 549. *System Parameter Constraints for epsilon Aurigae*. <http://adsabs.harvard.edu/abs/2010ApJ...714,549>
- Kambe, E., Sadakane, K., Hashimoto, O., Honda, S. and Sato, B. 2013 in *Helio- and Astero-seismology*, eds. H.Shibahashi and A.E. Lynas-Gray, ASP Conf. Ser. Vol.469, p.203. Line-profile Variations of the Primary of the Epsilon Aurigae Eclipsing Binary System. <http://adsabs.harvard.edu/abs/2013ASPC..479..203K>
- Kemp, J. C.; Henson, G. D.; Kraus, D. J.; Beardsley, I. S.; Carroll, L. C.; Ake, T. B.; Simon, T.; Collins, G. W. 1986 *Astrophys. Journal* 300, L11. <http://adsabs.harvard.edu/abs/1986ApJ...300L..11K>
- Kloppenborg, B., Stencel, R., Monnier, J. et al. 2015 *ApJ Suppl.* 220, 14 <http://adsabs.harvard.edu/abs/2015ApJS..220...14K>
- Lauterborn, D. 1970. *Astronomy and Astrophysics*, Vol. 7, p. 150 - 159. Evolution with mass exchange of case C for a binary system of total mass 7 M sun. <http://adsabs.harvard.edu/abs/1970A%26A.....7..150L>
- Mennickent, R. E. 2014 *PASP* 126, 821. *Evolutionary Stage of the Interacting Binary AU Mon*. <http://adsabs.harvard.edu/abs/2014PASP..126..821M>
- Sadakane, K., Kambe, E., Hashimoto, O., Honda, S. and Sato, B. 2013 *PASJ* 65, 1. Disk Origin Narrow Metallic Absorption Lines Observed during the 2009-2011 Eclipse of Aurigae. <http://adsabs.harvard.edu/abs/2013PASJ...65L...1S>
- Skumanich, A., Lopez Ariste, A. *The Astrophysical Journal*, 570:379386, 2002 May 1. The Physical Content of the Leading Orders of Principal Component Analysis of Spectral Profiles. <http://iopscience.iop.org/article/10.1086/339503/pdf>
- Stencel, R., 2012, *JAAVSO* 40, 618, ϵ Aurigae - an overview of the 2009-2011 Eclipse Campaign. <http://www.aavso.org/sites/default/files/jaavso/v40n2/618.pdf>
- Strassmeier, K., Weber, M.; Granzer, T.; Schanne, L.; Bartus, J.; Ilyin, I. 2014 *Astron Nachrichten* 335, 904. Time-series high-resolution spectroscopy and photometry of Aurigae from 2006-2013. <http://adsabs.harvard.edu/abs/2014AN....335..904S>

- Struve, O. and Elvey, C., 1930, Ap.J. 71: 136. Preliminary results of spectrographic observations of 7 epsilon Aurigae. <http://adsabs.harvard.edu/abs/1930ApJ....71..136S>
- Turner, Jake D.; Christie, Duncan; Arras, Phil; Johnson, Robert E.; Schmidt, Carl. 2016 Monthly Notices of the Royal Astronomical Society, Volume 458, Issue 4, p.3880-3891. Investigation of the environment around close-in transiting exoplanets using CLOUDY. // <http://adsabs.harvard.edu/abs/2016MNRAS.458.3880T>
- van Rensbergen, W.; de Greve, J. P.; Mennekens, N.; Jansen, K.; de Loore, C., 2011 Astron. Astrophys. 528, 16. Mass loss out of close binaries. The formation of Algol-type systems, completed with case B RLOF. // <http://adsabs.harvard.edu/abs/2011A&A...528A..16V>
- Wang, S.-i., Hildebrand, R., Hobbs, L., Heimsath, S., Kelderhouse, G., Loewenstein, R., Lucero, S., Rockosi, C., Sandford, D., Sundwall, J., Thorburn, J. and York, D. 2003, in M. Iye and A. F. M. Moorwood, editors, Instrument Design and Performance for Optical/Infrared Ground-based Telescopes, Volume 4841 of Society of Photo- 43 Optical Instrumentation Engineers (SPIE) Conference Series, pages 1145-1156. An echelle spectrograph for the Astrophysical Research Consortium (ARC) 3.5m telescope. doi: 10.1117/12.461447.ARCES

<https://arxiv.org/abs/1612.05287> v2